VALIDATION OF THE ARROTTA CODE AGIANST EXPERIMENTAL RBMK CRITICAL FACILITY DATA

B.R. Sehgal, H.W. Cheng and A. Romas
Royal Institute of Technology
Nuclear Power Safety, S-100 44 Stockholm, Sweden
sehgal@ne.kth.se; cheng@ne.kth.se; antanas@ne.kth.se

ABSTRACT

The work presented in this paper is on validation of the ARROTTA code against the experimental data obtained in a RBMK critical facility established in the Kurchatov Institute (KI). The ARROTTA code was developed for analysis of light water reactors (LWRs) cores, but not for RBMK-type reactors which differ from LWRs in core, fuel, and control rod designs. The RBMK critical facility design was designed based on the prototype of a RBMK power reactor. The size of the entire critical facility is 450x450 cm in base dimensions, and 410 cm high. The critical facility consists of 18x18 graphite stacks constructed with 25x25 cm graphite blocks. A number of zero-power experiments were carried out with different configurations in this RBMK critical facility. During all the experiments, radial and axial power distributions were measured by using copper foils or fission chambers. In some experiments, control rods were rapidly dropped into the active core, and the reactivity worths of the control rods were determined through the inverse kinetics. Numerical simulations of these experiments have been performed with the ARROTTA code. The CASMO-4 code was used to generate cross sections for fuel assembles while the WIMS-D4 code was employed for cross section generation for non-fuel assemblies such as control rods, additional absorbers, control rod imitators and reflector. The CASMO code is not capable of performing multi-assembly calculations. It is found that all the calculated results are in excellent agreement with the corresponding measured values providing, thus, a validation for the ARROTTA code.

1. INTRODUCTION

It is well known that the ARROTTA code was developed, exclusively for analysis of light water reactors (LWRs) cores, but not for RBMK-type reactors which differ much from LWRs in core, fuel, and control rod designs. Since the inception of application of the ARROTTA code in utilities, it has been subjected to significant validation efforts for LWRs. During the past few years, ARROTTA has been employed for the RBMK core safety research, but its validation work for RBMK-type reactors has not, so far, been carried out as comprehensively as for LWRs. The objective of the work presented in this paper is to validate the ARROTTA code against the experimental data obtained in the experiments performed in a RBMK-type in a RBMK-type critical facility (CF) which was built in the Kurchatov Institute (KI).

The RBMK critical facility was designed based on the prototype of a RBMK power reactor. The size of the entire critical facility is 450x450cm^2 in base dimension, and 410cm high. The critical facility consists of various types of channels, whose contents may be changed as needed. The

critical facility consists of 18x18 graphite stacks constructed with 25x25cm^2 graphite blocks. The critical facility details will be described below.

A number of zero-power experiments have been carried out with different core configurations in this RBMK critical facility. The data measured in the experiments performed included (1) positions of control rods to achieve criticality, (2) neutron fluxes including radial and axial flux distributions and (3) control rod reactivity worth. In this paper, three representative experiments were selected and analyzed with the ARROTTA code.

2. DESCRIPTION OF THE CRITICAL FACILITY

The RBMK Critical Facility was constructed at the Kurchatov Institute. Its design was based on the prototype of a RBMK power reactor. The size of the whole critical facility is 450x450cm^2 in base dimension, and 410cm high. It consists of 18x18 graphite stacks in a radial plane. These graphite stacks are assembled with rectangular 25x25cm^2 graphite blocks having 11.4cm diameter cylindrical openings in the center. Axially, it contains a top graphite reflector, the core and a bottom graphite reflector as shown in Figure 1.

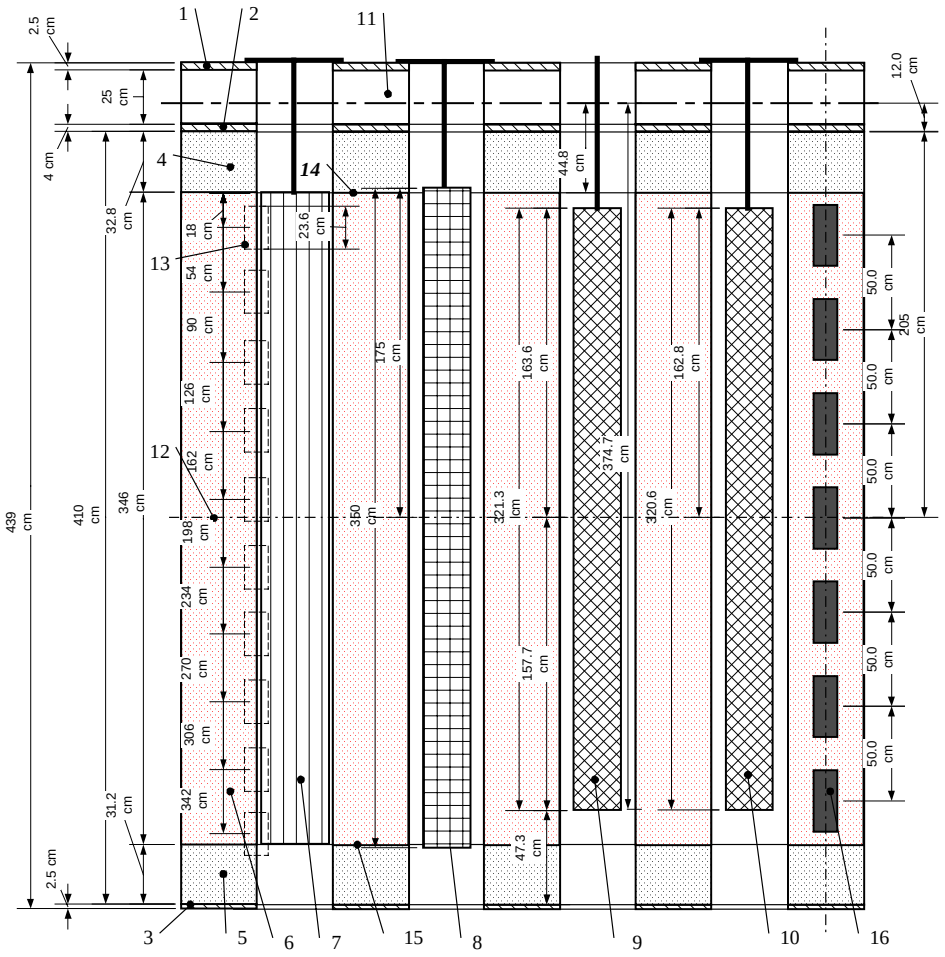

1- boron-polythene plate, 2-aluminium plate, 3-steel plate, 4-top graphite reflector, 5-bottom graphite reflector, 6-graphite that is in active core, 7-fuel assembly (fuel pellets stack), 8-additional absorber (AA), 9-fully inserted control rod (CR.), 10-control rod imitator (CRY), 11-reference point of control rod position indicator (PI), 12-central line of graphite stack, 13-position of copper foils for neutron flux measurements, 14-top of the active core, 15-bottom of the active core, 16-axial position of KNK-5 fission chambers

Figure 1. The Schematic of the Critical Facility

Channel tubes are placed vertically in the openings of graphite stacks, and separated from graphite blocks by graphite rings. The dimensions of a channel tubes are the same as those in RBMK-type reactor channels. However, the material of channel tubes in the critical facility is different from that in a RBMK power reactor. Aluminum alloy is used as the material of the critical facility channel tubes instead of zirconium-niobium alloy employed in channel tubes of a RBMK reactor.

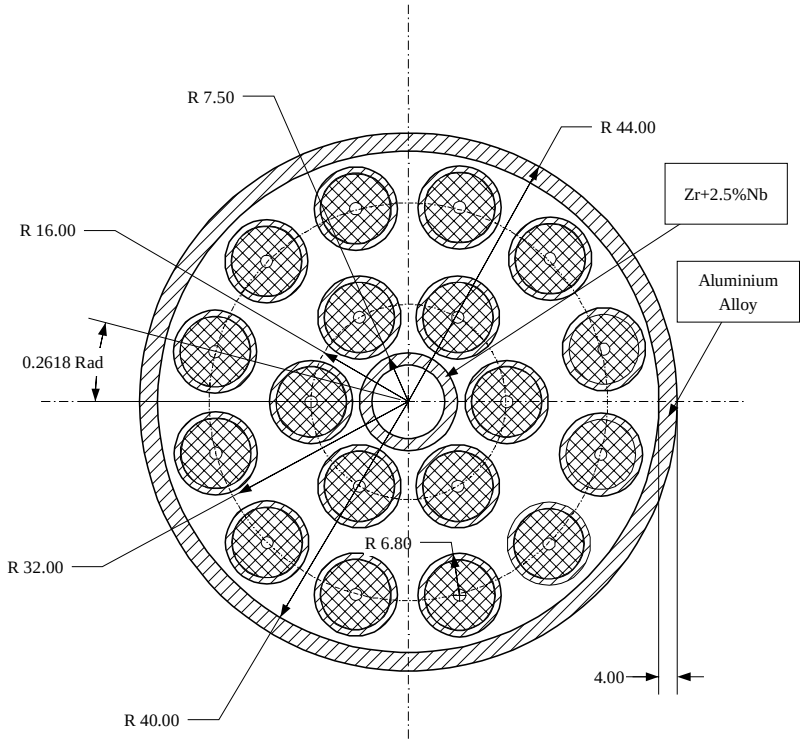

Figure 2. The Fuel Cluster in the Fuel Channel

Fuel assemblies, additional absorbers, control rods and control rod simulators are loaded inside the channels. The fuel assemblies used in the critical facility experiments are of the same design as those employed in a real RBMK reactor core. The geometry of the fuel bundles loaded in the channel is shown in Figure 2. Most of fuels used in the experiments are enriched to 2.0% by weight, while some are to 2.4%. The fuel channels, optionally, can be dry or filled with water, depending on the goals of the experiments.

Additional absorbers are employed in some experiments. The geometry of additional absorbers is shown in Figure 3, where a stainless steel tube supports a boron-steel absorber tube. The stainless steel tube is sealed on both ends. The boron-steel absorber tube is 350 cm long, and contains 2.0% boron by weight. In some experiments, water may surround the absorber tube. A control rod (CRD) in the critical facility contains three cylindrical sections of the same size and of the same material. They are joined together by aluminum rings. Each cylindrical section includes two concentric aluminum tubes, and the space between them is filled with natural B_4C (see Figure 3). The length of each section is 96.2 cm. The control rod channels are usually not filled with water for all the experiments performed. The position indicator (PI) indicates an axial position of a control rod in the core. A starting point of the indicator is 12 cm above the top of graphite stack. The tolerance of the position indicator is ±2.5 cm.

Generally, the design of control rod imitators (CRI) is similar to that of control rods. However, they are not movable in the core like additional absorbers. They are also about one centimeter shorter than normal control rods. The top of CRI stays 162.8cm above the mid-plane of graphite stacks (see Figures 1 and 3). The CRI channels may be filled with water in some experiments.

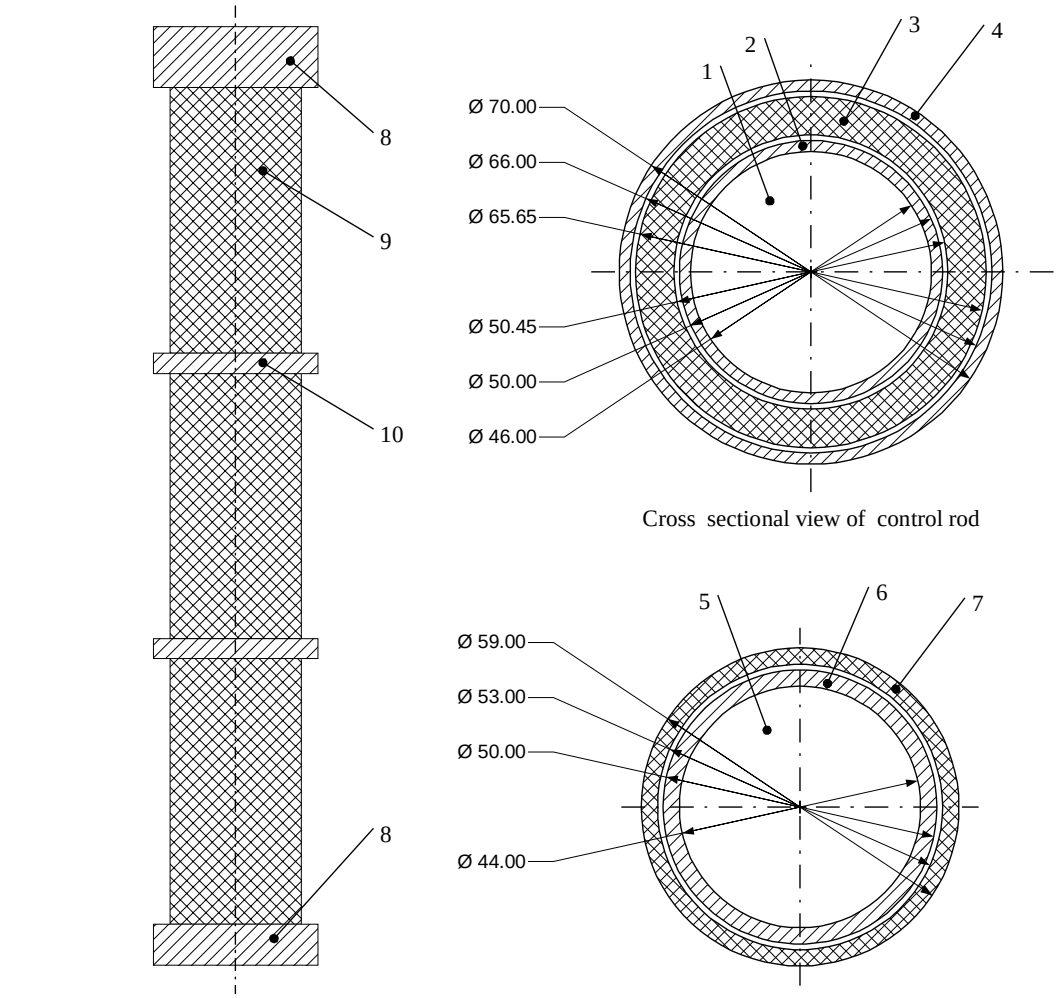

1-inner cavity that is filled with air (for CRI might be water), 2-inner aluminium tube, 3-absorber (B_4 C), 4-outer aluminium tube, 5-hermetically sealed inner cavity filled with air, 6-carrying stainless steel tube, 7- boron-steel (2.0% boron) absorber, 8-plugs, 9-absorber parts, 10-junctions

Figure 3. Schematics of Control Rod and Additional Absorber

3. INSTRUMENTATION IN THE CRITICAL FACILITY

For measuring neutron fluxes, either copper foils or fission chambers are implemented in the experiments performed. The copper foils are 23.6×1.5×0.03cm in size, and are placed in the periphery of the fuel cluster during the experiments. The axial locations of these foils are shown in Figure 1. The accuracy of this method varies between 1.5% and 7% [1]. There are as many as 54 fission chambers which are evenly distributed in the middle-plane of the core. In two channels, there are seven detectors positioned every 0.5m in the axial direction, as shown in Figure 1. In total, 68 sensors are placed in special channels located in the corners of graphite blocks.

Reactivity is determined by employing a PIR-4 reactimeter. The reactimeter accumulates signals from four ionization chambers distributed in the core, and performs the inverse point kinetics calculations to determine reactivity. The accuracy of reactimeter (not considering errors due to neglect of space effects, but only taking instrumentation error into account) is about 1-2% in the case of a small reactivity change (less than 0.25$), and 5-6% for a larger reactivity change [1].

4. SIMULATIONS OF EXPERIMENTS

4.1 GENERATION OF CROSS SECTIONS

To validate the ARROTTA code, three representative experiments were selected to be simulated with this code. The basis for the selection is that the core loading maps for these experiments are similar to those in prototypic RBMK cores. The cross sections for the various types of assemblies encountered in these four experiments are generated, employing two well-known lattice-physics codes, namely, CASMO-4 and WIMS-D_4. The CASMO-4 code was used to generate the cross sections for the fuel assemblies while the WIMS-D_4 code was employed for the non-fuel assemblies such as graphite reflector, control rod and additional absorber, since CASMO-4 is incapable of performing 3×3 multi-assembly calculations so far.

When calculating cross-sections of fuel assemblies by CASMO-4, it was assumed that all the compositions of the critical facility remain at the constant temperature of 300K. The boundary between thermal and fast energy groups was defined as 4 ev. The 'mirror' boundary condition was employed for single-assembly calculations. The fuel compositions include 2.0% or 2.4% U^{235}, U^{238}, U^{234} (0.02% of metallic uranium) and U^{236} (0.1% of metallic uranium). The fuel is assumed to be fresh without any fission products, such as Xe^{135} and Sm^{149}, since the facility is operated at cold zero power and only for short time periods. The graphite used as moderator in the critical facility contains some isotopes having large absorption, e.g., natural cadmium (15×10^{-5} w/%) and boron (15×10^{-5} w%), which must be taken into account. The exact mass fractions for these additional isotopes are not available, but the range of their variations in concentration is provided in reference 1. Their mass fractions are in the range of 25±3% with respect to the provided values as suggested by measurements performed.

When employing the WIMS-D_4 code to generate cross-sections for control rod channels, additional absorber channels and control rod imitator channels, a multi-assembly model is employed, in which eight fuel assemblies surround a non-fuel assembly. The mirror boundary condition was employed again. As for cross section generation for top, bottom and radial reflectors, only one fuel assembly is assumed to be in contact with the reflector. The 'zero-current' boundary condition was taken in this case.

4.2 MODELLING OF EXPERIMENTS WITH THE ARROTTA CODE

In the ARROTTA simulations of the three experiments, the whole core is divided into 18×18×21 rectangular nodes. One assembly stands for one node, and 21 nodes are used to represent the entire axial height. The first and last axial nodes are the top and bottom reflectors, respectively. The zero-flux boundary condition is employed for all six boundaries of the critical facility. Since the power generated in the experiments is negligibly small, fuel and moderator temperature feedbacks are not taken into account. Six delayed neutron groups are introduced in this the calculations.

Comparison of results involves three aspects. One aspect is regarding comparison of effective multiplication factors. Since the critical facility in these four experiments is maintained critical by maneuvering control rods in the beginning of the experiments, the calculated effective multiplication factors have to be compared to unity. The second aspect is to deal with the comparison of neutron flux distributions calculated by ARROTTA with those measured in the experiments. In first two experiments, the relative neutron flux distributions are derived from the measurements of the activities of the copper foils irradiated in the core. For comparison, the activities of the copper foils are also calculated with the two-group flux distributions produced by ARROTTA. In order to estimate the activities of the copper foils, the two-group fluxes for the positions, where copper foils are positioned in the experiments, should be interpolated using

the average nodal neutron fluxes calculated by ARROTTA. The activities of the copper foils are determined by the relative absorption reaction rates in the copper foils, as shown in the equation below:

$$A_\alpha = \Phi_1 \cdot \sigma_{a_1} + \Phi_2 \cdot \sigma_{a_2} \tag{1}$$

where A_a stands for the relative activity of the copper foil, and Φ_1 and Φ_2 are fast and thermal neutron fluxes , respectively while σ_{a1} and σ_{a2} stand for fast and thermal microscopic absorption cross sections of copper, respectively. The cross sections of copper were generated by CASMO-4. Finally, the calculated relative copper foil activities are normalized, and compared with the measured values. Unlike the first two experiments, fission chambers are employed to measure fluxes in the last two experiments. Since fast neutrons produce very few fission reactions compared to those produced by thermal neutrons, only calculated thermal neutron fluxes are compared with those measured by fission chambers. Similarly, the thermal neutron fluxes for the positions where fission chambers are placed in the experiments should be calculated simply by averaging the thermal fluxes of four surrounding nodes. For comparison, The thermal fluxes, both calculated and measured, are normalized for comparison purposes.

The third aspect is concerned with comparison of reactivity induced due to withdrawal or insertion of control rods. The calculation of reactivity is based on the inverse point kinetics theory, taking advantage of the signals from different detectors, as shown in Equation 2:

$$\rho(t) = 1 + \frac{L}{\beta}\frac{d\ln T(t)}{dt} - \frac{1}{T(t)}\sum_{i=1}^{6}\frac{\beta_i}{\beta}e^{-\lambda_i t}\left(T_0 + \lambda_i\int_0^t T(t')e^{\lambda_i t'}dt'\right) \tag{2}$$

where $T(t)$ is the amplitude of the signal detected during the transient, and T_0 stands for the amplitude of the signal detected at the initial critical condition. L/β is taken as 0.2 from reference [1]. The effective delayed neutron fractions β_i and the decay constants λ_I, and are taken from reference [2]. The terms $T(t)$ and T_0 are expressed as follows:

$$T(t) = \frac{\Phi_D(t)}{\overline{\Phi}_C(0)} \qquad T_0 = \frac{\Phi_D(0)}{\overline{\Phi}_C(0)} \tag{3}$$

where $\Phi_D(t)$ is the neutron flux calculated for the location of detectors during the transients, $\Phi_D(0)$ stands for the neutron flux at the initial critical condition, and $\Phi_C(0)$ is the average core neutron flux calculated at the initial critical condition.

4.3 RESULTS OF SIMULATIONS AND COMPARISONS

4.3.1 Experiment 1

The core configuration of the first experiment is shown in Figure 4. There are 192 fuel assemblies, twenty of which contain additional stainless steel spacers with the same amount of steel as in the upper section of a normal RBMK-1500 fuel bundle. The fuel and additional absorber channels are both filled with water of 300 K. The system pressure is 1 bar. This core also includes four control rods, three of which, namely, P15-10, P9-16 and P3-14, are fully inserted, and another called P5-8, is inserted 150 cm in the core. The radial neutron fluxes were measured by irradiating copper foils and measuring their activities. The copper foils are placed 162 cm below the top of the active core as shown in Figure 1. The radial positions of the copper foils are indicated in Figure 4. The results of comparison are presented in Figure 5. The average discrepancy in copper activities is only 4.05%, and the maximum error is 8.3%. The axial neutron flux distribution was measured in the channels P10-8 and P15-8, where the axial location of the copper foils is indicated in Figure 1. The axial neutron fluxes calculated and

measured for these two channels are compared in Figure 6. The effective multiplication factor calculated at the critical conditions is 1.00410.

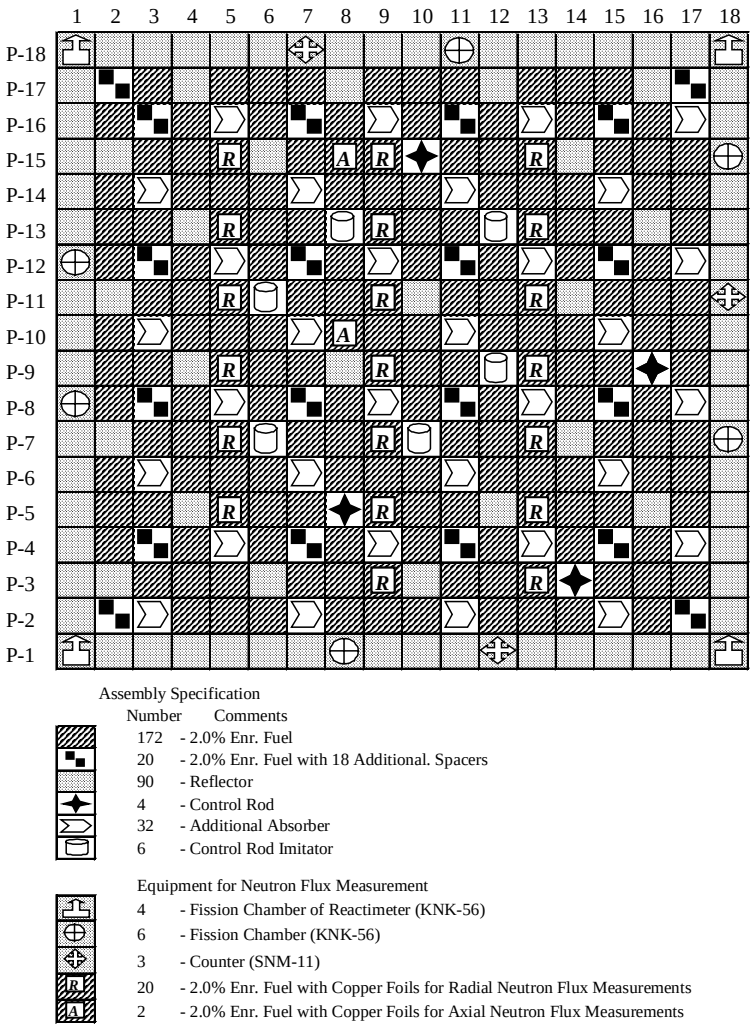

Figure 4. The Configuration of Experiment 1

	75.7	53.8	64.3		91.4	118.7	128.5	- Measured
P-15	79.6	50.6	63.2	P-7	95.4	117.0	127.1	- Calculated
	5.1%	-6.0%	-1.7%		4.4%	-1.4%	-1.1%	- Discrepancy
	90.8	76.9	77.2		104.9	133.0	123.1	
P-13	95.9	75.1	73.6	P-5	109.6	137.0	121.9	
	5.7%	-2.3%	-4.7%		4.5%	3.0%	-1.0%	
	87.3	139.0	112.2			90.9	59.2	
P-11	89.1	136.7	109.1	P-3		98.4	59.3	
	2.0%	-1.6%	-2.8%			8.3%	0.2%	
	116.5	153.0	103.1		5	9	13	
P-9	117.0	149.6	94.8					
	0.5%	-2.2%	-8.1%					
	5	9	13					

Figure 5. Comparison of Radial Neutron Fluxes for Experiment 1

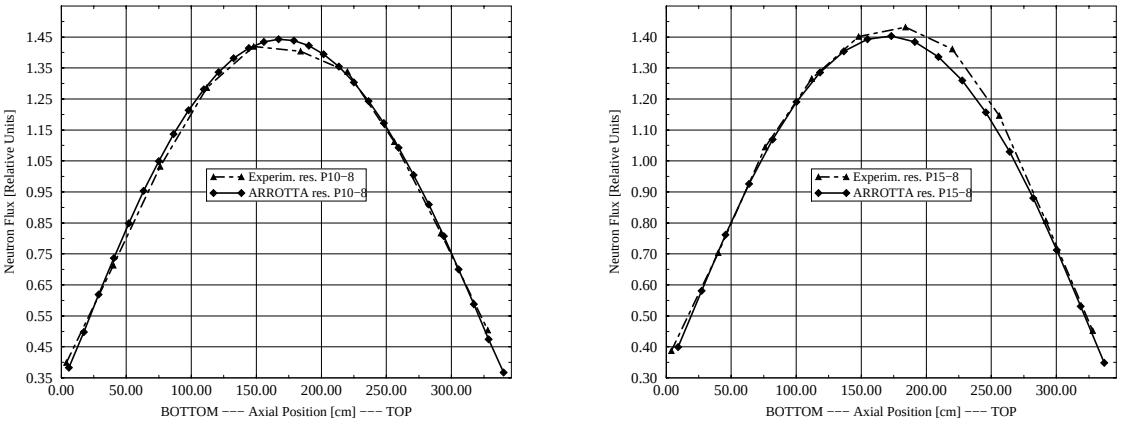

Figure 6. Comparison of Axial Neutron Profiles
for Channels P10-08 (Left) and P-15-08 (Right) in Experiment 1

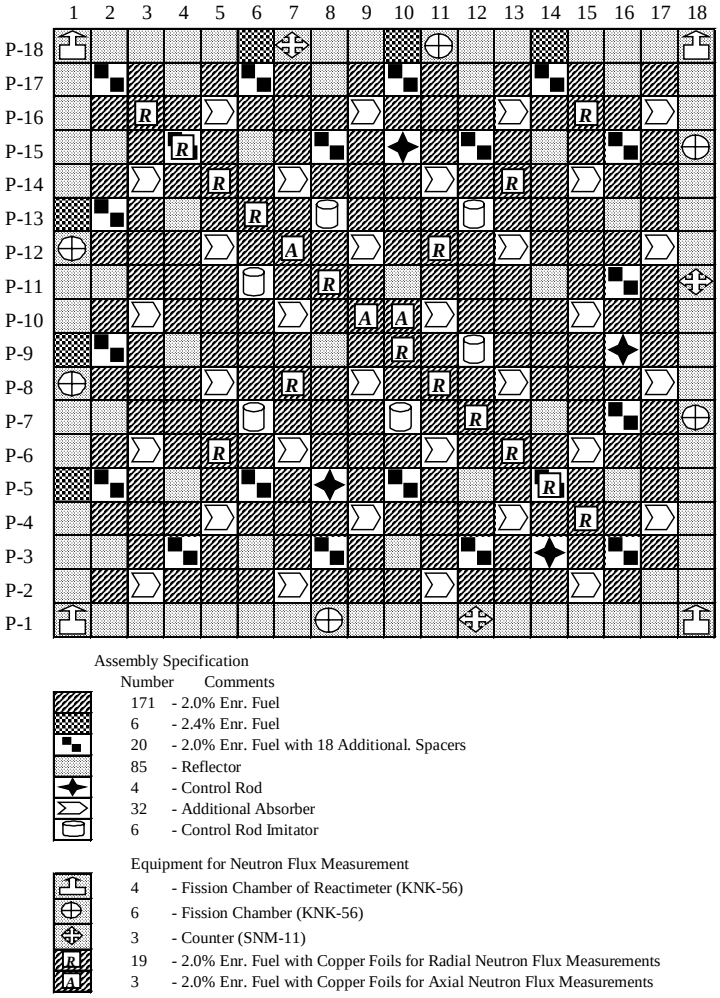

Figure 7. The Core Configuration of Experiment 2

4.3.2. Experiment 2

The core Configuration of Experiment 2 is shown in Figure 7 where 191 fuel assemblies with 2.0% enrichment and 6 fuel assemblies with 2.4% enrichment are loaded. All the fuel and

additional absorber channels are filled with water. The control rods P5-8, P9-16, and P3-14 are fully inserted, and P15-10 is inserted 205 cm according to the position indicator. The effective multiplication factor calculated at the critical conditions is 1.00293. The measurements of the

Table 1. Comparison of the Calculated and Measured Radial Neutron Fluxes for Experiment 2

Coordinate	Measured Flux (RU)	Calculated Flux (RU)	Discrep. [%]	Coordinate	Measured Flux (RU)	Calculated Flux (RU)	Discrep. [%]
P16-03	49.0	53.1	8.27%	P16-15	60.0	58.7	-2.16%
P15-04	79.0	82.7	4.68%	P06-05	73.0	78.3	7.23%
P14-05	105.0	109.9	4.67%	P08-07	111.0	111.1	0.12%
P13-06	104.0	103.7	-0.33%	P09-10	126.0	124.9	-0.87%
P12-07	102.0	97.6	-4.33%	P08-11	103.0	98.0	-4.84%
P11-08	127.0	125.0	-1.60%	P07-12	103.0	105.5	2.39%
P10-09	152.0	149.6	-1.56%	P06-13	106.0	113.3	6.89%
P10-10	139.0	139.5	0.37%	P05-14	80.0	85.7	7.15%
P12-11	129.0	118.8	-7.89%	P04-15	52.0	54.9	5.49%
P14-13	99.0	89.8	-9.29%				

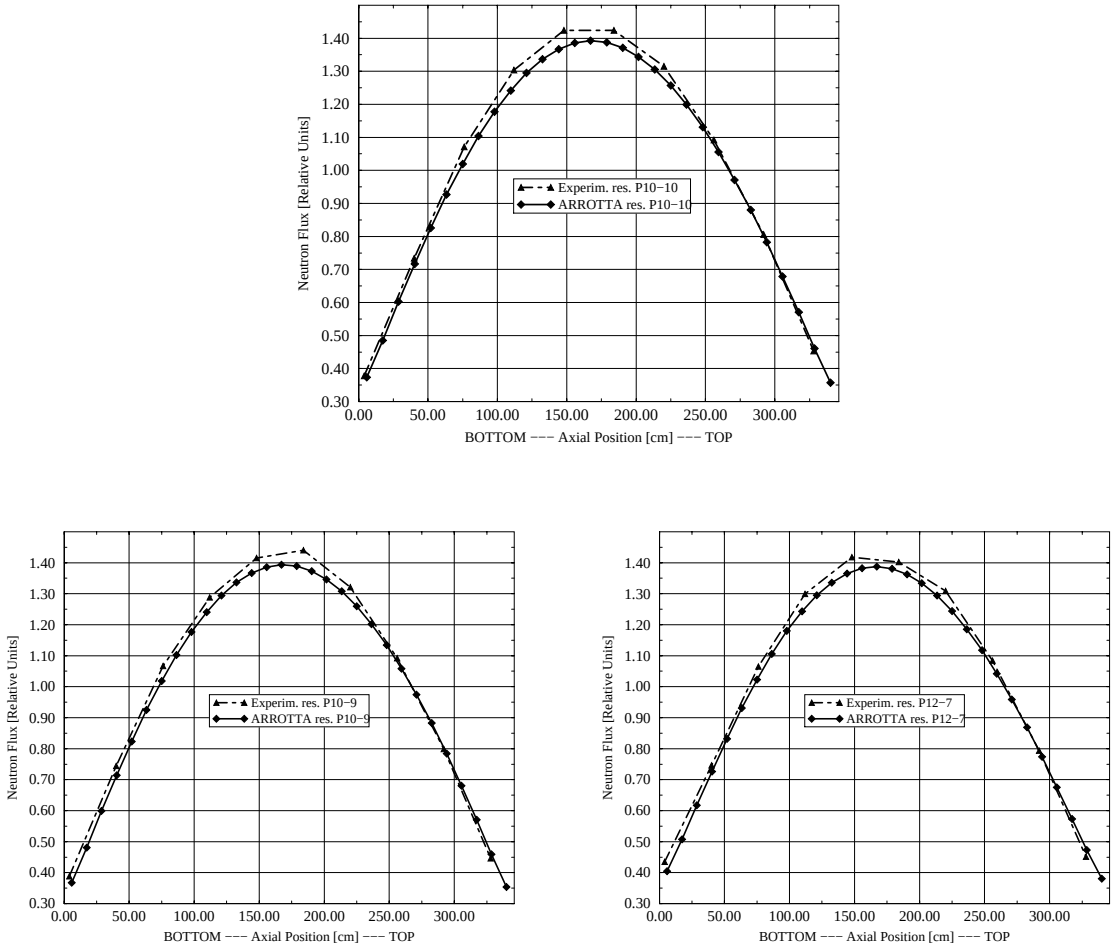

Figure 8. Comparison of Axial Neutron Flux Profiles
for Channels P10-10, P10-09 and P12-07 in Experiment 2

radial neutron flux were performed in 19 fuel channels (see Figure 7) on the plane which is 162 cm below the top of active core. The results of comparison of the calculated and measured

radial neutron fluxes for 17 fuel channels are listed in Table 1. It is seen that the average discrepancy is about 5.4%, and the maximum error is up to 9.3%. The axial neutron fluxes ware measured in Channels P10-9, P10-10, and P12-7. They are shown in Figure 8, and compared with those calculated by ARROTTA.

4.3.3. Experiment 3

Experiment 3 was performed in the configuration shown in Figure 9. This core consists of 192 fuel assemblies with 2.0% enrichment, 172 of which do not contain additional spacers, but 20 of which do. The core also contains 32 additional absorbers and six control rod imitators. In this configuration, there are 22 control rods, called AZ, KO and MR. However, only MR and KO are activated during the experiments. So, only 15 control rods were moved, and 7 AZ control rods were kept out of the core during the course of these two experiments. The AZ channels function just as graphite blocks with aluminum tubes. The channels containing fuel assemblies and additional absorbers are filled with water. The other channels are dry.

The neutron fluxes were measured by employing KNK-5 fission chambers (for this reason this experiment is called EFC Experiment in the following figures). The chambers were placed at the vertices of the graphite blocks in the special openings. Two chains of seven chambers were applied for measuring axial flux distributions, and 54 chambers were located in the mid-plane of the core for measuring radial power distributions as seen in Figures. 1 and 9.

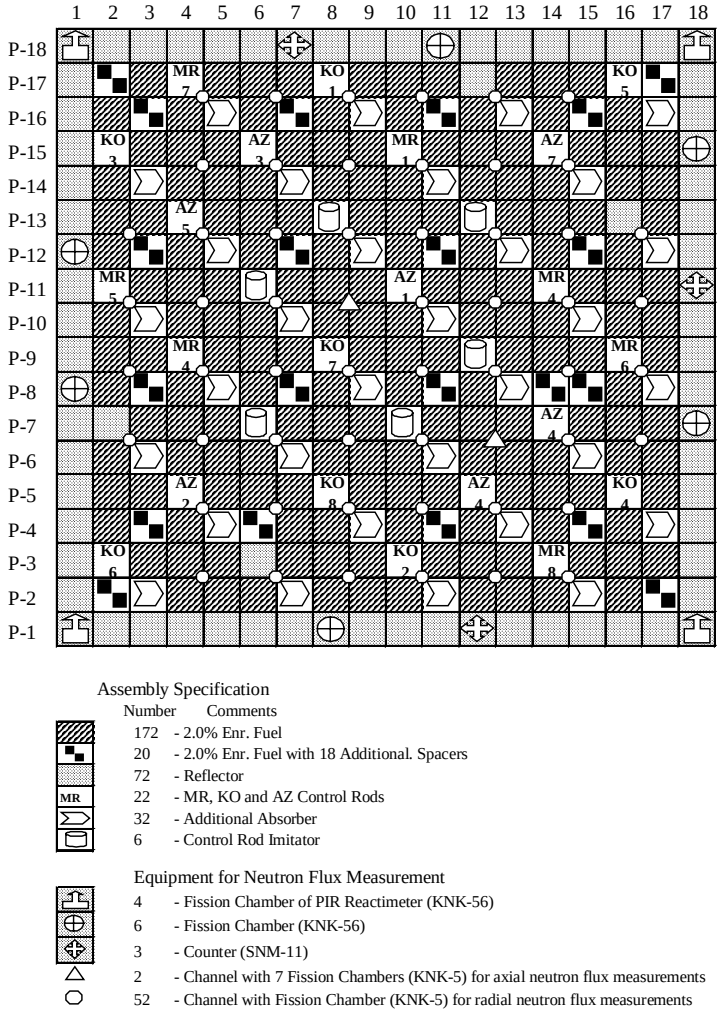

Figure 9. The Critical Assembly Configuration Employed during Experiments 3

The reactivity was determined by employing a reactimeter during rod-dropping transients. The reactimeter collects the signals from four KNK-56 ionization detectors that are located in the corners of the critical facility as shown in Figure 9. Axially, they were fixed in the mid-plane of the core. For some cases, the reactivity was determined by summation of the signals from all of the 68 KNK-5 fission chambers. In the course of Experiment 3, four control rods were dropped into the core at a velocity of 180 cm/sec after the critical facility reached criticality by adjusting the positions of the control rods. The critical positions of control rods for Experiment 3 are described in Table 2. The radial and axial neutron fluxes were measured at the initial critical conditions, at 3 and 15 seconds after the initiation of control rod drop.

Table 2. Description of CRDs in Experiment 3

CRD Activated	CRD Fully Inserted	CRD Partially Inserted	CRD Fully Withdrawn
KO-3, MR-4, MR-5, 7	MR-1, MR-6, MR-8	KO-8 (195cm)	MR-3,4,5,7, KO-1,2,3,4,5,6,7

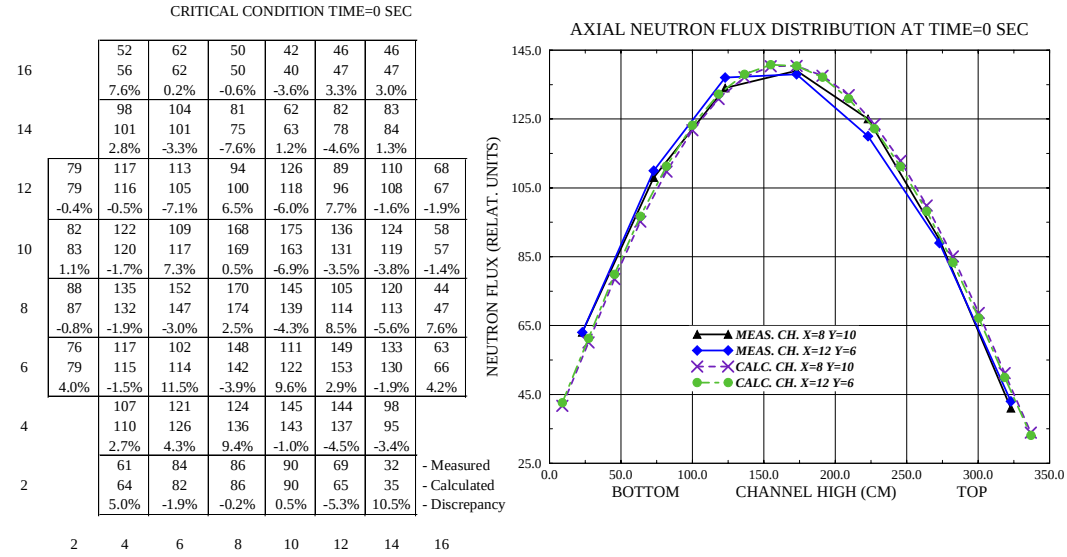

Figure 10. Comparisons of Radial and Axial Flux distributions at 0 Second in Experiment 3

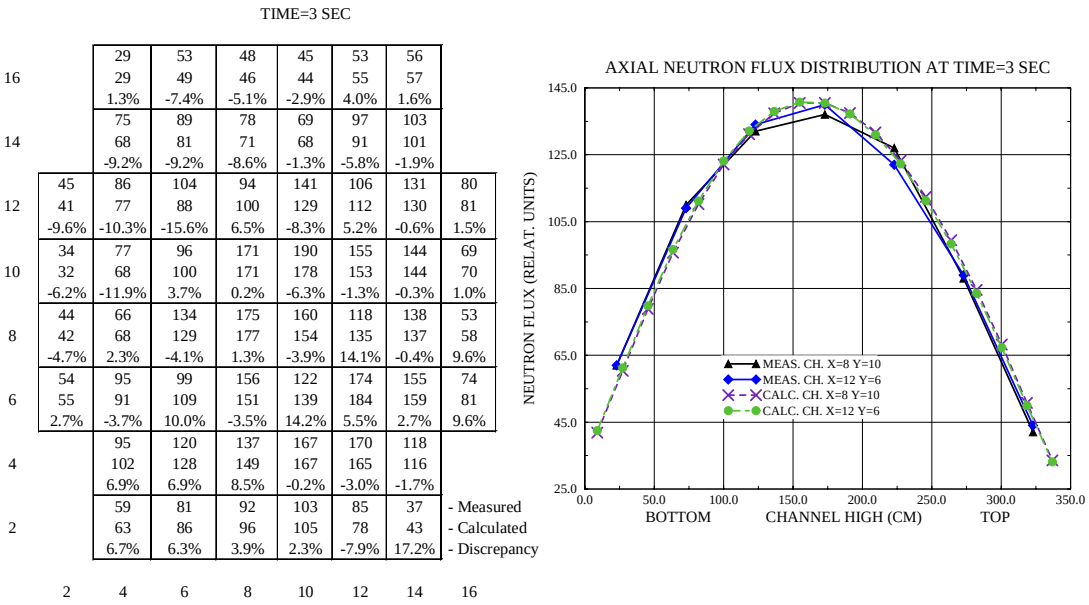

Figure 11. Comparisons of Radial and Axial Flux distributions at 3 Seconds in Experiment 3

Figure 10 shows the results of comparisons of the measured radial and axial flux distributions calculated with those calculated by ARROTTA at 0 second in Experiment 3. Similarly, The results of comparisons are also presented in Figures 11 and 12 at 3 and 15 seconds, respectively. It is indicated that average discrepancy in neutron flux with respect to the measured value is 3.9% at 0 second, and increases to 5.5% and 5.1% at 3 and 15 seconds. As shown at the left-hand sides of Figures 10, 11 and 12, the calculated axial flux distributions for two different channels are all in rather good agreement with those measured. In addition, the effective multiplication factor calculated at the initial critical conditions is 1.0029.

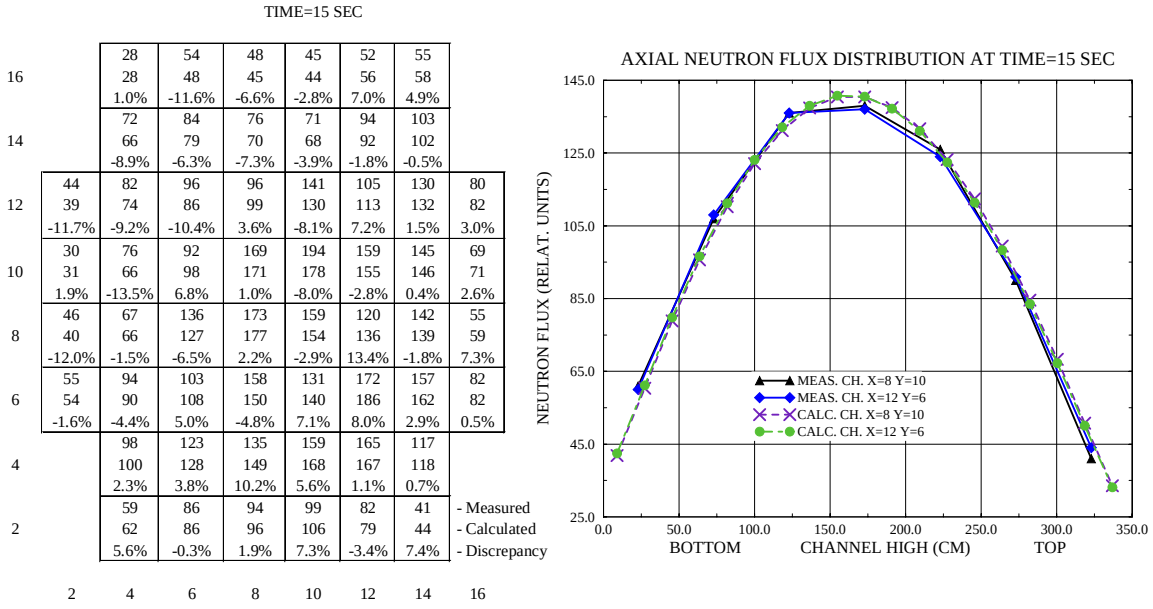

Figure 12. Comparisons of Radial and Axial Flux distributions at 15 Seconds in Experiment 3

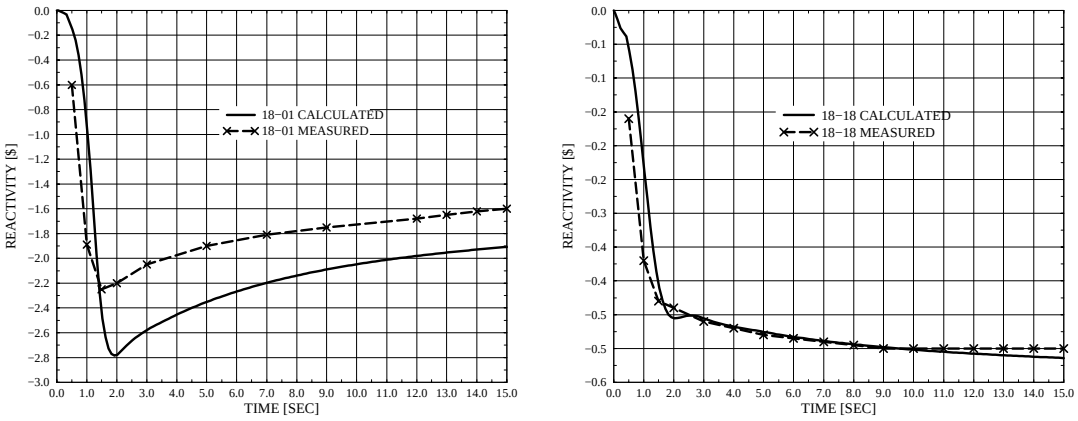

Figure 13. Comparisons of Calculated and Measured Reactivities
for Channels P18-01 and P18-18

As mentioned above, the reactivity was obtained with the sum of the signals from KNK-56 ionization chambers, recorded during the control rod drop transient, through the inverse kinetics theory as expressed in Equation 2. All the results of the comparisons of the calculated and measured reactivities are presented in Figures 13 and 14. Figure 13 shows the comparisons of the reactivity derived from the data obtained from two separate chambers located in P18-01 and

P18-18 channels. It is found that there is a better agreement between calculated and measured reactivities at the location of chamber P18-18. The discrepancy is larger for the detector P18-01. The reactivity calculated by the sum of the signals is close to that measured as shown in Figure 13. It is indicated from Figure 14 that the measured reactivity is -0.76β while the calculated one is about -0.78β.

It should be noted that accuracy of reactivity calculations depends strongly on the number and positions of detectors in the core. As indicated in Figure 12 or Figure 13. The reactivity differs in amplitude and shape for different chambers by analyzing the signals from individual chambers. The sum of the signals from at least four chambers should be employed for the reactivity estimations during the transient.

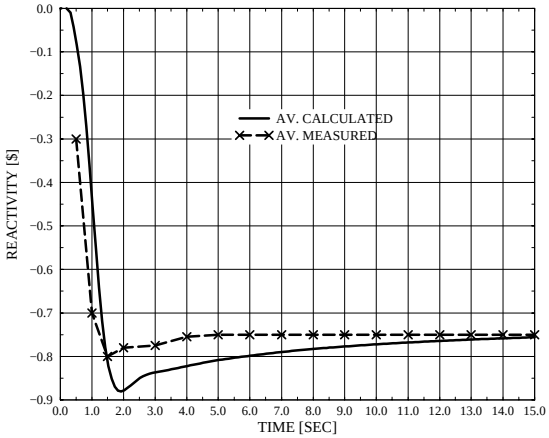

Figure 14. Comparisons of Reactivities Calculated from the Sum of Signals of Four Detectors

CONCLUSIONS

In general, the results calculated by the ARROTTA code are in good agreement with those measured for three experiments described in this paper. Table 3 summarizes the overall results of the comparisons for these experiments. It is seen that the effective multiplication factors, calculated at the initial critical core configurations, are quite close to unity although greater than unity. For the comparisons of the calculated radial fluxes with the measured values, the discrepancy varies between 1 and 5% at the initial critical configurations. However, the discrepancy increases up to 11% for the control rod transient (Experiment 3). Table 3 also gives the calculated and measured reactivities. It is seen that they are in good agreement as well.

Table 3. Summary of Comparison of ARROTTA Results with Experimental Data

Experiment		Keff Calculated	Average Discrepancy in Radial Flux	Reactivity Measured	Reactivity Calculated
1		1.00410	4.05%	--	--
2		1.00293	5.35%	--	--
3	0 s	1.00290	3.91%	-0.76β	-0.78β
	3 s	-	5.55%		
	15 s	-	5.11%		

In addition, it is expected that the ARROTTA results would be improved when only one lattice code such as HELIOS, which is capable of generating cross sections for fuel and non-fuel assembles, is employed instead of using the combination of CASMO and WIMS-D4 employed in this paper. Finally, it may be concluded that the ARROTTA code is an excellent candidate code for analyzing RBMK-type reactors.

REFERENCES

1. G.B. Davydoya and V.M. Kachanov, “The Experiments on the Critical Assembly of RBMK Initial Data for Computer Modeling,” Moscow, 1995.

2. A. Krayushkin, A.V. Afanasieva, M.N. Babystev, G.B. Davydova, A.V. Glemborsky, A.M. Fedosov, and S.M. Tsareva, “Code Assessment for RBMK Reactor Applications. Assessment of the STEPAN Computer Code for RBMK Neutronic Modeling, Stage 2: The Development of the Documentation on the STEPAN Code and on Verification and Validation Existed. The Full Scale Neutronic Code STEPAN,” Moscow, 1998.

3. A. Krayushkin, G.B. Davydova, Yu A. Tishkin, A.V. Glemborsky, S.M. Tsareva, and L.N. Zaharova, “Code Assessment for RBMK Reactor Applications. Assessment of the STEPAN Computer Code for RBMK Neutronic Modeling, Stage 3: The Development of the Benchmark Documentation. Documentation on Benchmarks for 3-D RBMK Neutron Kinetics Validation,” Moscow, 1998.